Article

Ag$_2$O Nanoparticles-Doped Manganese Immobilized on Graphene Nanocomposites for Aerial Oxidation of Secondary Alcohols

Mohamed E. Assal [1], Mohammed Rafi Shaik [1] , Mufsir Kuniyil [1,2] , Mujeeb Khan [1], Abdulrahman Al-Warthan [1], Mohammed Rafiq H. Siddiqui [1,* and Syed Farooq Adil [1,*

[1] Department of Chemistry, College of Science, King Saud University, P.O. Box 2455, Riyadh 11451, Saudi Arabia; mhd.elshahat@gmail.com (M.E.A.); rafiskm@gmail.com (M.R.S.); mufsir@gmail.com (M.K.); kmujeeb@ksu.edu.sa (M.K.); awarthan@ksu.edu.sa (A.A.-W.)

[2] Department of Chemistry, Koneru Lakshmaiah Education Foundation, Vaddeswaram, Guntur 522502, Andhra Pradesh, India

* Correspondence: rafiqs@ksu.edu.sa (M.R.H.S.); sfadil@ksu.edu.sa (S.F.A.); Tel.: +966-11-467-0439 (S.F.A.)

check for
updates

Abstract: Ag$_2$O nanoparticles-doped MnO$_2$ decorated on different percentages of highly reduced graphene oxide (HRG) nanocomposites, i.e., (X%)HRG/MnO$_2$–(1%)Ag$_2$O (where X = 0–7), were fabricated through straight-forward precipitation procedure, and 400 °C calcination, while upon calcination at 300 °C and 500 °C temperatures, it yielded MnCO$_3$ and manganic trioxide (Mn$_2$O$_3$) composites, i.e., [(X%)HRG/MnCO$_3$–(1%)Ag$_2$O] and [(X%)HRG/Mn$_2$O$_3$–(1%)Ag$_2$O], respectively. These nanocomposites have been found to be efficient and very effective heterogeneous catalysts for selective oxidation of secondary alcohols into their respective ketones using O$_2$ as a sole oxidant without adding surfactants or nitrogenous bases. Moreover, a comparative catalytic study was carried out to investigate the catalytic efficiency of the synthesized nanocomposites for the aerobic oxidation of 1-phenylethanol to acetophenone as a substrate reaction. Effects of several factors were systematically studied. The as-prepared nanocomposites were characterized by TGA, XRD, SEM, EDX, HRTEM, BET, Raman, and FTIR. The catalyst with structure (5%)HRG/MnO$_2$–(1%)Ag$_2$O showed outstanding specific activity (16.0 mmol/g·h) with complete conversion of 1-phenylethanol and >99% acetophenone selectivity within short period (25 min). It is found that the effectiveness of the catalyst has been greatly improved after using graphene support. A broad range of alcohols have selectively transformed to desired products with 100% convertibility and no over-oxidation products have been detected. The recycling test of (5%)HRG/MnO$_2$–(1%)Ag$_2$O catalyst for oxidation of 1-phenylethanol suggested no obvious decrease in its performance and selectivity even after five subsequent runs.

Keywords: silver oxide nanoparticles; secondary alcohols; catalyst; graphene; oxidation

1. Introduction

Catalytic oxidation of alcohols into their respective carbonyls such as aldehydes and ketones is of crucial importance in synthetic chemistry [1]. Aldehyde and ketone derivatives are employed as high value intermediates and precursors in several industries, such as perfumery, vitamins, cosmetics, confectionary, flavors, insecticides, aniline dyes, flame-retardants, and agro-processing [2,3]. Conventionally, oxidation of alcohols was performed by using expensive, polluting, and hazardous stoichiometric amount of oxidizing reagents (e.g., CrO$_3$, SeO$_2$, NaClO, KMnO$_4$, PCC, Na$_2$Cr$_2$O$_7$, RuO$_4$, and Br$_2$) [4,5]. However, there are disadvantages to using these oxidants, such as high cost and

the production of large amounts of toxic waste, which largely reduce their industrial applications. Recently, huge efforts have been devoted to developing more green catalytic protocols to reduce the disadvantages of conventional oxidation approaches [6]. Therefore, the use of environmentally friendly oxidants like molecular O_2 has received growing interest for the alcohol oxidation from the viewpoint of green chemistry, because O_2 is cheap, natural, abundant, and generates innocuous by-products (H_2O and H_2O_2) [7]. Several catalytic protocols for alcohol oxidation using O_2 as a clean oxidizing agent have developed and exhibited high performance [8]. In the last several years, a plethora of studies have used noble metals like palladium [9], platinum [10], gold [11], and ruthenium [12] as efficient catalysts for selective alcohol oxidation. In addition to their high costs, these noble metals also suffer from some drawbacks due to difficulties in synthesis, and the rarity of these precious metals make these catalysts impractical for industry [13]. Consequently, considerable efforts have been devoted to replacing these precious catalysts with inexpensive and plentiful non-noble metals or transition metals such as V [7], Cu [14], Ni [15], Co [16], Fe [17], Zr [18], and Zn [19]. Additionally, the metal or metal oxide NPs-based catalysts were reported as highly effective for selective alcohol oxidation. Furthermore, it has been broadly reported that the efficiency of metal NPs significantly improved upon doping with other metals owing to the metallic NPs have huge surface area [20]. Among different types of metal oxides, MnO_2 has been found to be the most stable metal oxide which has superior properties [21], such as high activity, highly specific capacitance and is an eco-friendly material [22]. Hence, Mn-containing catalysts have been extensively applied as highly effective catalysts for the catalytic oxidation of alcohols [23].

　　　Graphene, a unique crystal of an individual layer of sp^2 hybridized carbon atoms, was densely packed into a 2D honeycomb lattice [24]. Single graphene sheet is known as the strongest material ever measured [25]. In 2004, the individual sheet of graphene was experimentally isolated for the first time via mechanical exfoliation of graphite; a plethora of studies have been reported on graphene due to the extraordinary properties and numerous applications since that date [26]. Graphene is an amazing material, which received widespread interest owing to the fact it has huge surface area (2630 m^2/g), superior corrosion resistance, exceptional thermal conductivity (5000 $W \cdot m^{-1} \cdot K^{-1}$), high electron mobility (250,000 cm^2/Vs), high chemical stability, ultrathin thickness, and highly electrically conductive (6000 $S \cdot cm^{-1}$) [27]. However, the preparation of single-crystalline, defect-free, single-layer graphene is still a challenge. The exceptional optical, catalytic, electronic, and magnetic properties of graphene based metal nanocomposites have been exploited in many industrial applications such as supercapacitor, touch screens, batteries, sensors, solar cells, and catalysis [27]. Therefore, huge efforts have devoted to combine uniformly different types of nanomaterials, including metallic NPs with graphene or its derivatives, which remarkably improved the properties of these materials; this is probably due to the synergistic effect between the graphene and NPs [28]. Besides enhancing their properties, the metal NPs also behave as a stabilizing agent against the agglomeration of single graphene layers [29]. Moreover, the combination of metal NPs with graphene also assisted the exfoliation of single graphene sheets [30]. Graphene and its derivatives are widely utilized as a promising supporting material for metallic NPs due to their superior features, e.g., huge surface area, superior chemical stability, and simple reusability of metals from spent catalysts [31]. To exploit these fascinating properties of graphene in catalysis, it is necessary to produce large quantity of the graphene by using graphene oxide (GO) and HRG [32]. GO consists of myriad oxygenic functionalities on the basal plane such as hydroxyl, carboxyl, epoxy, and carbonyl groups [33], to promote the oxidation reaction [31]. GO can reduced to highly reduced graphene (HRG) via chemical or thermal reduction reactions [34]; most of oxygenated functionalities in GO layer can be reduced and left behind as numerous topological defects and carbon vacancies [35]. Recently, HRG has received growing attention as a promising material for catalyst supports in the oxidation of several organic substrates [36], maybe due to the fact that the HRG surface behaved as the anchoring site for the aromatic alcohols and oxygen on the surface by π–π stacking near the metal NPs [36]. This advantage, together with its extremely specific surface area, offers HRG excellent

catalyst support in the selective oxidation process [30]. In general, catalytic active metallic NPs with smaller particle size usually showed higher catalytic activity owing to their extremely high surface area and increased active exposed sites [37]. However, owing to their small size, metal NPs are not stable and readily agglomerated because of their high surface energy, which reduces their catalytic performance and stability [38]. In order to solve this problem, researchers found that immobilizing catalytically active sites onto supports could be a suitable solution [37]. As expected, in the current study the catalyst with graphene support exhibited higher reactivity than that without graphene support. Graphene-based metal NPs have been found to be efficient catalysts for numerous organic transformations, such as Suzuki coupling [39], reduction of alcohols [40], preparation of aniline [41], oxidation of ammonia borane [42], and oxidation of methanol [43]. Especially, graphene-supported metal NPs were broadly applied as a heterogeneous catalyst for the selective oxidation of alcohols into their corresponding carbonyl compounds, e.g., Pd/GC [44], MnO_2/GO [45], Au/RGO [46], Pd/HRG [47], and Au/GQDs/Fe_3O_4 [48].

In connection with our efforts in the utilization of several metallic oxide NPs as effective catalysts for the liquid-phase oxidation of alcohols using oxygen [22,49,50], we compare between the catalytic efficiency of Ag_2O NPs-doped MnO_2 without using graphene support (HRG) and the catalytic performance after using HRG as a catalyst support toward the oxidation of 1-phenylethanol in order to understand the support effect (Scheme 1). The prepared nanocomposites were fabricated, and their catalytic performances examined in aerial oxidation of alcohols via ideal green methodology, i.e., using a green oxidizing agent while being free of any base or surfactants. The as-obtained nanocomposites have characterized by XRD, TGA, SEM, EDX, HRTEM, BET, Raman, and FT-IR.
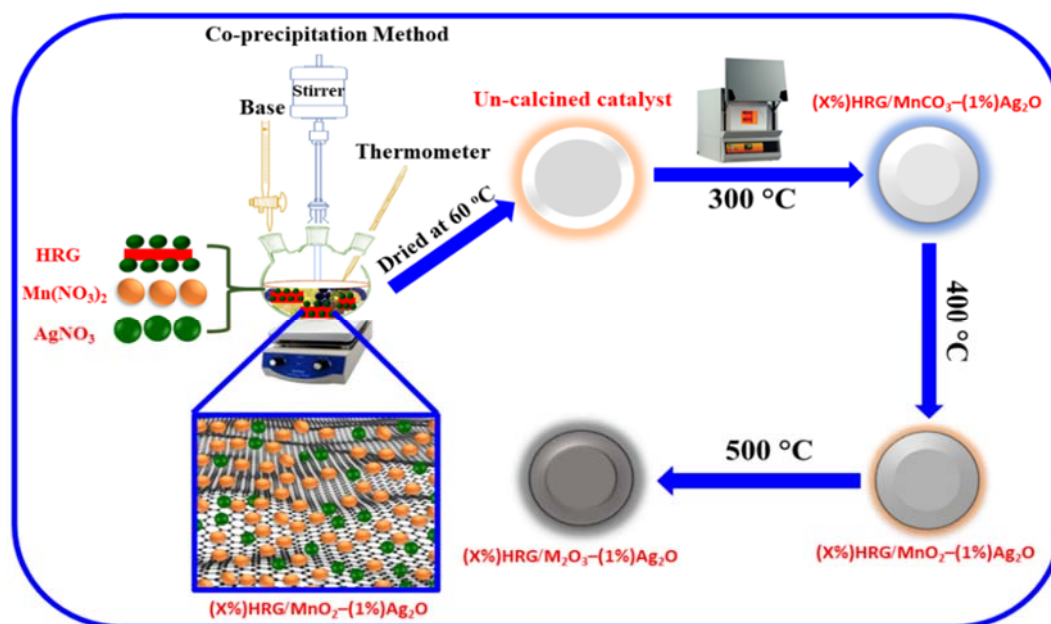
Scheme 1. Schematic depiction for the fabrication of (X%)HRG/$MnCO_3$–(1%)Ag_2O, (X%)HRG/MnO_2–(1%)Ag_2O, and (X%)HRG/Mn_2O_3–(1%)Ag_2O nanocomposites.

2. Materials and Methods

2.1. Preparation of HRG

In the beginning, graphene oxide (GO) was prepared from pristine graphite by the Hummers procedure [51]. Then, GO has been reduced to HRG using hydrazine hydrate by following our earlier publication [52].

2.2. Preparation of (X%)HRG/MnO₂–(1%)Ag₂O Catalyst

(X%)HRG/MnO$_2$–(1%)Ag$_2$O nanocomposite was prepared via precipitation procedure (where X = 0, 1, 3, 5 and 7). In a typical preparation, stoichiometric amount of Mn(NO$_3$)$_2$·4H$_2$O, AgNO$_3$, and HRG were mixed in a round bottomed flask and subjected to ultrasonication for 0.5 h. After that, the solution was heated to 80 °C, while vigorously stirring using a mechanical stirrer and 0.5 M solution of NaHCO$_3$, and was added drop wise until the pH of solution reached 9 for 3 h; then the stirring continued over night at room temperature. The solution was filtered and dried, followed by calcination in muffle furnace at 300, 400, and 500 °C.

2.3. Catalyst Characterization

The as-obtained nanocomposites were characterized by various techniques such as XRD, TGA, SEM, EDX, HRTEM, BET, Raman, and FT-IR [52].

2.4. General Procedure for Oxidation of Alcohols

In a typical experiment, a mixture of the 1-phenylethanol (2 mmol), toluene (10 mL), and the catalyst (300 mg) was transferred in a glass three-necked round-bottomed flask (100 mL); the resulting mixture was then heated to desired temperature with vigorous stirring. The oxidation experiment was started by bubbling oxygen gas at a flow rate of 20 mL·min^{-1} into the reaction mixture. After the reaction, the solid catalyst was filtered off by centrifugation, and the liquid products were analyzed by gas chromatography to determine the conversion of the alcohol and product selectivity by (GC, 7890A) Agilent Technologies Inc. (Santa Clara, CA, USA), equipped with a flame ionization detector (FID) and a 19019S-001 HP-PONA column.

3. Results and Discussion

3.1. Catalyst Characterization

3.1.1. X-Ray Diffraction Analysis (XRD)

XRD analysis was carried out to investigate the crystallographic structure of the as-synthesized nanocomposite catalyst. Figure 1 displays characteristic XRD patterns of the graphite, GO, HRG, un-supported MnO$_2$–(1%)Ag$_2$O, and (5%)HRG/MnO$_2$–(1%)Ag$_2$O nanocomposite. The graphite's XRD pattern displayed a sharp diffraction signal at 2θ = 26.5°, with a d-spacing of 3.37 Å as exhibited in Figure 1a. The GO crystalline degree is moderately small with a wide-ranging typical diffraction band at approximately 2θ = 11.8°, which corresponds to the characteristic structure of GO as displayed in Figure 1b. The graphite peak at 2θ = 26.5° vanishing and the presence of a new band at 2θ = 11.8° designate the development of GO through graphite oxidation. This change principals to a rise in an inter-planar distance from 3.37 to 4.83 Å for graphite and GO, respectively, which might be ascribed due to the presence of several O-containing functional groups. The XRD diffraction of HRG nanosheets is noticed at around 2θ = 24.6° with (002) plane, which is a finger-print peak of HRG and diffraction peak at 2θ = 11.8 vanishing evidently, designating that GO is entirely reduced to HRG as exhibited in Figure 1c. The MnO$_2$–(1%)Ag$_2$O XRD pattern highly matches with the stated data of pyrolusite MnO$_2$ (JCPDS file No. 24-0735), while the nanocomposite (5%)HRG/MnO$_2$–(1%)Ag$_2$O shows a related XRD pattern as MnO$_2$–(1%)Ag$_2$O with HRG characteristic band at 2θ = 24.6°, specifying the existence of HRG in the as-synthesized nanocomposite (Figure 1e).
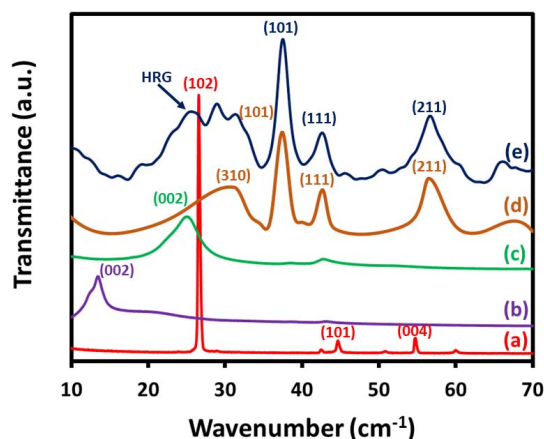
Figure 1. XRD analysis of (**a**) graphite, (**b**) GO, (**c**) HRG, (**d**) MnO$_2$–(1%)Ag$_2$O, and (**e**) (5%)HRG/MnO$_2$–(1%)Ag$_2$O.

3.1.2. Fourier Transforms Infrared Spectroscopy (FT-IR)

The FT-IR spectral analysis of GO, HRG, and (5%)HRG/MnO$_2$–(1%)Ag$_2$O nanocomposite is displayed in Figure 2. In the FT-IR spectrum of GO (Figure 2a), the absorption peak at 3440 cm^{-1} can be attributed to hydroxyl groups (–OH) stretching modes of (–COOH) groups and water molecules, the intense peak at 1740 cm^{-1} resembles (C=O) stretching of (−COOH), and the absorption strong peak at around 1630 cm^{-1} is allocated to the stretching vibration of carbon backbone (C=C/C−C) from unoxidized graphite lattice. Furthermore, the three peaks situated at 1395, 1225, and 1060 cm^{-1} can be ascribed to the stretching modes of (C−OH), (C−O−C), and (C−O), correspondingly. FT-IR spectrum of HRG (Figure 2b) displayed that the broad intense peak at 1215 cm^{-1} associated with (C−OH) stretching vibration and weak absorption peak at approximately 1636 m^{-1} is ascribed to (C=C) group, due to the skeletal aromatic vibration; additional peaks matching to oxygen comprising functional groups vanished when associated with GO. The (5%)HRG/MnO$_2$–(1%)Ag$_2$O nanocomposite FT-IR spectra evidently shows the whole reduction of maximum of oxygenated functional groups on the surface of GO (Figure 2c). The intense bands attributed to (C=O), (C−O−C), and (C−O) stretching vibrations at 1740, 1225, and 1060 cm^{-1} were not observed associated with GO, and the oxygen possessing functionalities on the GO plane are efficiently reduced. Moreover, a wide-ranging peak at 1634 cm^{-1} resultant to (C=C) stretching mode accredited to the skeletal aromatic vibration was witnessed (Figure 2c). Meanwhile, a sharp, intense absorption peak situated at 580 cm^{-1} is allocated to Mn−O vibrations in MnO$_2$.
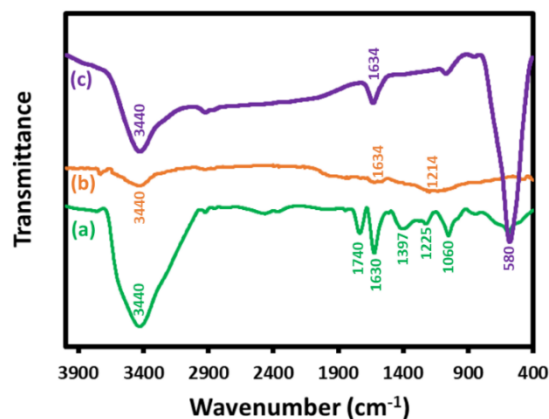
Figure 2. FT–IR analysis of (**a**) GO, (**b**) HRG, and (**c**) (5%)HRG/MnO$_2$–(1%)Ag$_2$O.

3.1.3. Thermogravimetric Analysis (TGA)

TGA analysis was conducted to study the thermal stability of graphite, GO, HRG, MnO_2–(1%)Ag_2O, and (5%)HRG/MnO_2–(1%)Ag_2O as shown in Figure 3. The TGA curves endorses the whole reduction of GO to HRG using hydrazine monohydrate as reducing agent. Figure 3a,b showed that the thermal stability of GO is much inferior to graphite. The pristine graphite TGA curve shows an entire weight loss of approximately 1% (Figure 3a). Moreover, GO displays ~6% weight loss nearby 100 °C, evidently due to the absorbed H_2O molecules loss and volatile compounds, followed by the highest weight loss of approximately 43% owing to the pyrolysis of the oxygenated carrying functional groups in the temperature range of 200–370 °C, and, finally, a weight loss of around 11% owing to the pyrolysis of the carbon skeleton, which is perceived in the temperature range of 370–800 °C. HRG thermogram (Figure 3c) displays an entire weight loss of less than 19% in the same temperature range, owing to the reduction of most of the oxygenated carrying functionalities. The (5%)HRG/MnO_2–(1%)Ag_2O displayed entire weight loss of nearly 17% in the identical temperature range (Figure 3e), which is marginally more than the weight loss apparent from the MnO_2–(1%)Ag_2O thermal degradation pattern, indicating efficient reduction of GO. As a consequence, it is established that the as-synthesized (5%)HRG/MnO_2–(1%)Ag_2O catalyst is stable up to 520 °C.
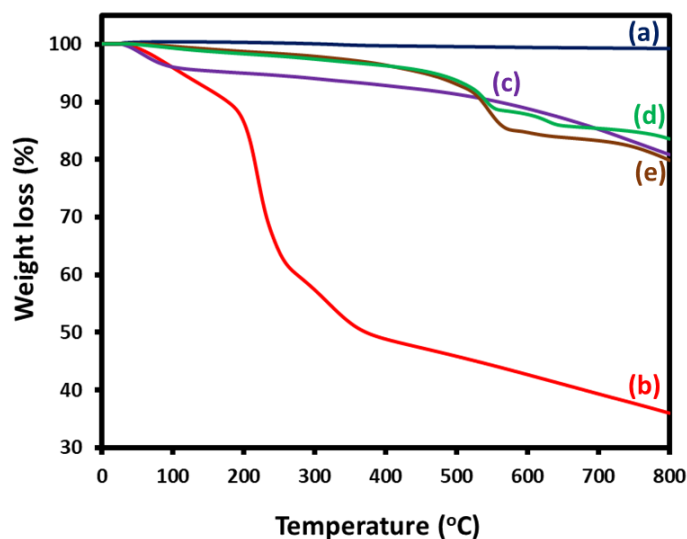
Figure 3. TGA graph of (**a**) graphite, (**b**) GO, (**c**) HRG, (**d**) MnO_2–(1%)Ag_2O, and (**e**) (5%)HRG/MnO_2–(1%)Ag_2O.

3.1.4. SEM and EDX

The size and morphology of the as-obtained (5%)HRG/MnO_2–(1%)Ag_2O nanocomposite was analyzed by SEM technique and associated with MnO_2–(1%)Ag_2O as displayed in (Figure 4). The MnO_2–(1%)Ag_2O catalyst displayed micro size but precise cuboidal shape particles; nevertheless, the (5%)HRG/MnO_2–(1%)Ag_2O nanocomposite (Figure 4b), remarkably, displays aggregation of rather smaller size crystals, which appear on the surface through proper surface nucleation/growth process. Furthermore, the elemental composition analysis of the as-prepared (5%)HRG/MnO_2–(1%)Ag_2O nanocomposite is also investigated through EDX analysis, as noticed in Figure 5. The presence of Ag, Mn, C, and O_2 is clearly specified in the EDX spectrum, and the percentage of composition is within the theoretical range.
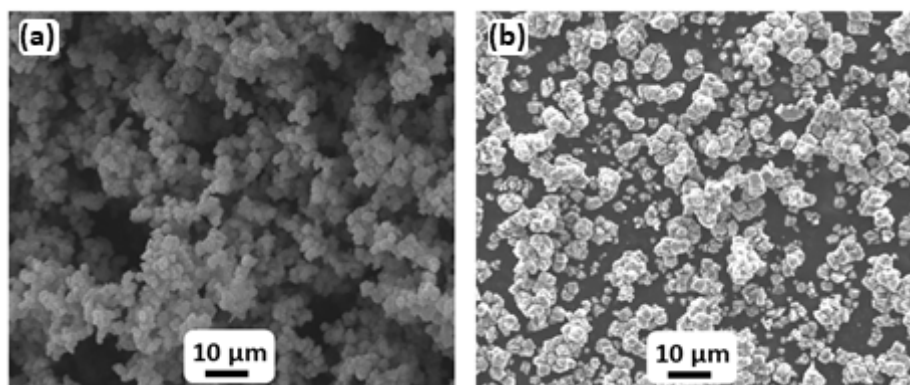
Figure 4. SEM images of (**a**) MnO_2–(1%)Ag_2O and (**b**) (5%)HRG/MnO_2–(1%)Ag_2O nanocomposite.

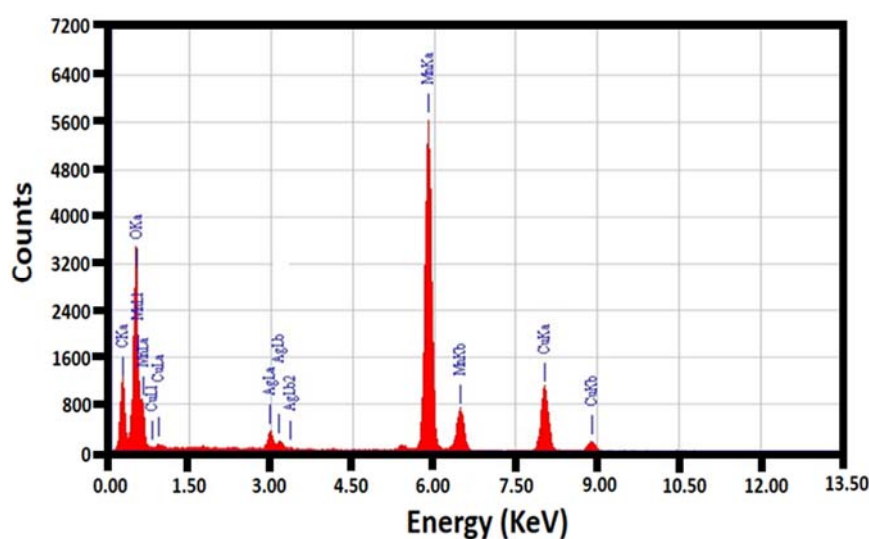**Figure 5.** EDX spectra of the (5%)HRG/MnO_2–(1%)Ag_2O nanocomposite.

### 3.1.5. High Resolution Transmission Electron Microscope (HRTEM)

HRG, MnO_2–(1%)Ag_2O, and (5%)HRG/MnO_2–(1%)Ag_2O nanocomposite morphology and size were examined using HRTEM. Figure 6a shows extremely exfoliated HRG nanolayers, which are thin, flake-like, silky, and transparent, whilst the HRTEM image of the (5%)HRG/MnO_2–(1%)Ag_2O nanocomposite clearly shows the nanosize of the Ag_2O in the catalyst with 0.95 ± 0.14 nm as average diameter with spherical shape, and is homogenously distributed on the crumpled HRG nanosheets, as illustrated in Figure 6d–f. Additionally, the HRTEM image of the MnO_2–(1%)Ag_2O catalyst (without graphene) displays the Ag_2O NPs of 2.16 ± 0.23 nm, which is larger than the Ag_2O NPs obtained by using graphene support. This can be possibly attributed to the graphene nanolayers reducing the aggregation of Ag_2O NPs (Figure 6b,c). Notably, the size of Ag_2O NPs in the (5%)HRG/MnO_2–(1%)Ag_2O nanocomposite is found to be smaller than that of the Ag_2O NPs in the catalyst without graphene support, i.e., MnO_2–(1%)Ag_2O (Figure 6c,f), that is, this may be the reason why (5%)HRG/MnO_2–(1%)Ag_2O nanocomposite showed enhanced efficiency compared to MnO_2–(1%)Ag_2O catalyst.
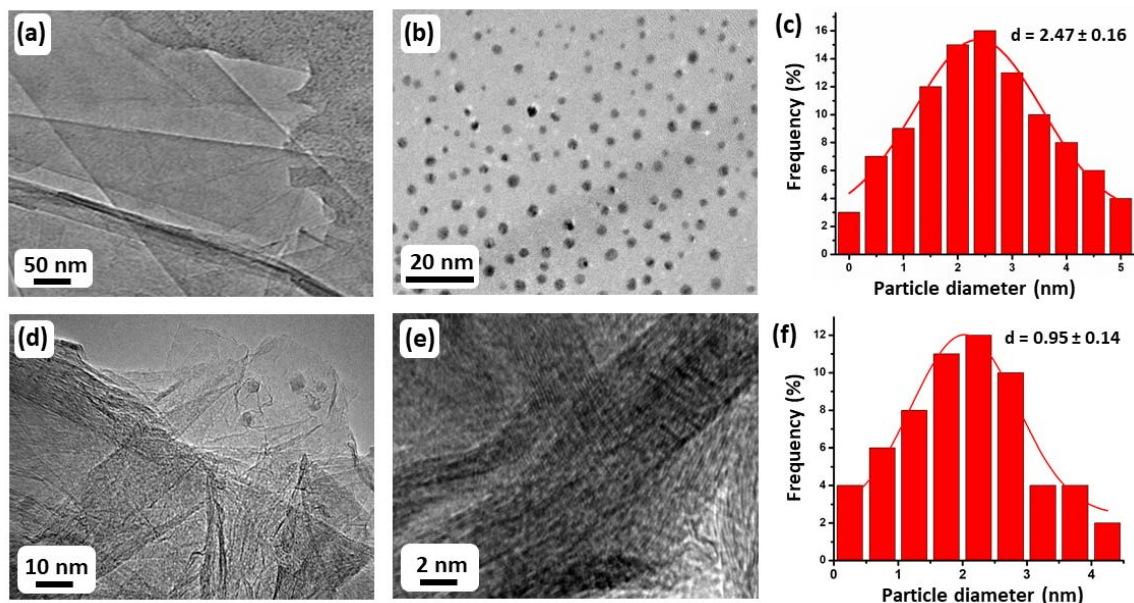
Figure 6. HRTEM images of (**a**) HRG, (**b**) MnO_2–(1%)Ag_2O, (**d,e**) (5%)HRG/MnO_2–(1%)Ag_2O, and (**c,f**) particle size distributions of MnO_2–(1%)Ag_2O and (5%)HRG/MnO_2–(1%)Ag_2O nanocomposite, respectively.

3.1.6. Raman Spectroscopy

Figure 7 exhibits the Raman spectrum of GO, MnO_2–(1%)Ag_2O, and (5%)HRG/MnO_2–(1%)Ag_2O nanocomposite. Raman spectra of the MnO_2–(1%)Ag_2O and (5%)HRG/MnO_2–(1%)Ag_2O nanocomposite (Figure 7b,c) demonstrate a characteristic peak situated at 642 cm^{-1}, confirming the existence of MnO_2 in both MnO_2–(1%)Ag_2O and (5%)HRG/MnO_2–(1%)Ag_2O nanocomposite. Additionally, the presence of HRG support in the (5%)HRG/MnO_2–(1%)Ag_2O nanocomposite is confirmed by the existence of two characteristic peaks at ~1591 and 1337 cm^{-1} correspondingly, commonly denoted as D-band and G-bands. The G and the D bands in GO spectrum are shifted and located at 1605 and 1346 cm^{-1} (Figure 7a), which is due to the destruction of the sp^2 character by the oxidation of graphite to GO and existence of oxygen-possessing functional groups on the GO plane. The G peak in (5%)HRG/MnO_2–(1%)Ag_2O is shifted by ~14 cm^{-1} from 1605 to 1591 cm^{-1}, while a slight shift is noticed in the D peak from 1346 to 1337 cm^{-1}, indicating an efficient reduction of GO to HRG. Interestingly, the obtained observations are very much in accordance with the XRD results.
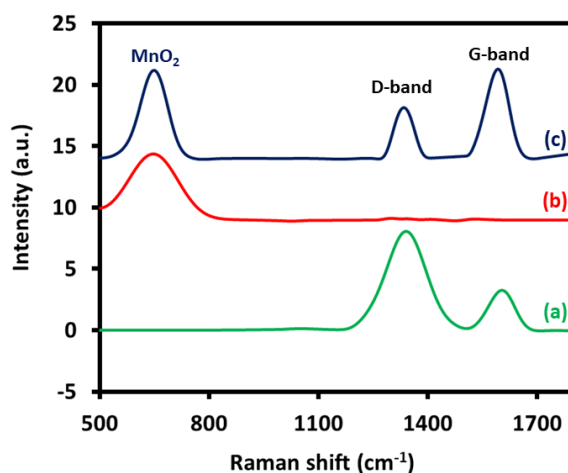

Figure 7. Raman analysis of (**a**) GO, (**b**) MnO_2–(1%)Ag_2O, and (**c**) (5%)HRG/MnO_2–(1%)Ag_2O nanocomposites.

3.1.7. BET Surface Area

BET surface area analysis of the as-obtained catalysts was determined, to compare the changes in surface area due to calcination at various temperatures and the existence of HRG in the catalytic protocol and to understand the correlation between the surface areas of the synthesized materials and the effectiveness of the catalytic protocol for alcohol oxidation. Table 2 displayed that the surface areas of the fabricated catalysts (without graphene), i.e., $MnCO_3$–(1%)Ag_2O, MnO_2–(1%)Ag_2O, and Mn_2O_3–(1%)Ag_2O, are about 52, 84, and 42 m^2/g, respectively, whereas the surface areas of the prepared catalyst after doping it with HRG at various temperatures (300 °C, 400 °C, and 500 °C), i.e., (5%)HRG/$MnCO_3$–(1%)Ag_2O, (5%)HRG/MnO_2–(1%)Ag_2O, and (5%)HRG/Mn_2O_3–(1%)Ag_2O, increased to 107, 149, and 99 m^2/g, respectively. As anticipated, the catalytic performance after loading HRG on the catalyst, i.e., (5%)HRG/$MnCO_3$–(1%)Ag_2O, (5%)HRG/MnO_2–(1%)Ag_2O, and (5%)HRG/Mn_2O_3–(1%)Ag_2O, was also increased.

3.2. Catalytic Studies

To explore the catalytic efficiency of the synthesized nanocomposites, oxidation of 1-phenylethanol using molecular O_2 as a clean oxidant was employed as a representative example (Scheme 2). Different catalysts were synthesized by altering the wt. % of HRG in the catalyst and calcination treatment. Additionally, the effect of catalyst quantity, temperature, and reaction time on the effectiveness of the synthesized catalysts is studied in detail.
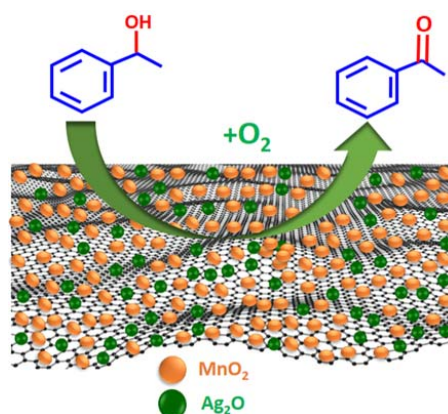
Scheme 2. Schematic depiction of oxidation of 1-phenylethanol into acetophenone catalyzed by the as-fabricated catalyst.

3.2.1. Impact of HRG Support

The performance of the oxidation catalyst can be improved using graphene or its derivatives as a catalyst support [42,43,53]. From our previously reported study, it was found that Ag_2O NPs was found to be an excellent promoter to the MnO_2 catalyst, and the MnO_2–Ag_2O(1%) catalyst exhibited highest catalytic activity [54]. Herein, the catalyst MnO_2–(1%)Ag_2O was selected and further developed by addition of different percentages of HRG in order to fine-tune its performance. Firstly, we have studied the catalytic efficiency of pure, highly reduced graphene oxide for the aerobic oxidation of 1-phenylethanol using O_2 as an oxidizing agent at 100 °C. It was found that HRG alone is not active for this oxidation process (Table 1, entry 1). Several catalysts with changing weight percentages of HRG, i.e., (0–7%) HRG in the nanocomposite, were synthesized and examined in terms of their activities for 1-phenylethanol oxidation. The results revealed that the catalysts (1%)HRG/MnO_2–(1%)Ag_2O and (3%)HRG/MnO_2–(1%)Ag_2O display alcohol conversion of 69.81% and 91.34%, respectively, within 25 min of reaction time at 100 °C (Table 1, entries 3, 4). By raising the wt.% of HRG in the catalyst, the conversion of 1-phenylethanol was also increased, and the (5%)HRG/MnO_2–(1%)Ag_2O yielded 100% conversion along with 16.0 mmol/g·h specific activity, which is highest performance

among all other HRG percentages (Table 1, entry 5). Further increase of the weight percentage of HRG led to decrease in the performance of the catalyst; this is may be due to high percentage of HRG support, which led to the blocking of the active sites of the catalyst (Table 1, entry 6). Interestingly, the MnO_2–(1%)Ag_2O catalyst without HRG support gave only 60.39% conversion under identical circumstances (Table 1, entry 2).

Table 1. The catalytic properties of various catalysts for the aerial oxidation of 1-phenylethanol.

Entry	Catalyst	Conversion (%)	Specific Activity (mmol/g·h)	Selectivity (%)
1	HRG	3.94	0.63	>99
2	MnO_2–(1%)Ag_2O	60.39	9.66	>99
3	(1%)HRG/MnO_2–(1%)Ag_2O	69.81	11.17	>99
4	(3%)HRG/MnO_2–(1%)Ag_2O	91.34	14.61	>99
5	(5%)HRG/MnO_2–(1%)Ag_2O	100.0	16.0	>99
6	(7%)HRG/MnO_2–(1%)Ag_2O	84.45	13.51	>99

Note: Conditions: 2 mmol of 1-phenylethanol, 300 mg catalyst, 400 °C calcination temperature, and 20 mL/min oxygen rate at 100 °C for 25 min.

Therefore, it could be deduced that the support (HRG) played a fundamental role in enhancement of the efficiency of the present catalytic protocol. The effectiveness of the (5%)HRG/MnO_2–(1%)Ag_2O nanocomposite is much higher than that of MnO_2–(1%)Ag_2O nanocatalyst, possibly due to the increase in the adsorption of the reactant aromatic alcohols onto HRG surface through π–π interaction near the Ag_2O NPs attached on the HRG layers, in addition to graphene support having huge surface area that can homogenously disperse the active sites (Ag_2O–MnO_2 NPs). Moreover, the existence of carbon defects and oxygen carrying functionalities on HRG surface anchored the Ag_2O NPs and prevented the aggregation of graphene sheets. The product selectivities toward acetophenone stayed motionless (>99%) throughout all processes (Table 1, entries 1–6). The obtained data are collected in Table 1 and are depicted in Figure 8. Thus, it can be deduced that the (5%)HRG/MnO_2–(1%)Ag_2O nanocomposite exhibited highest efficiency among the all-prepared nanocomposites, and therefore it is selected in the later studies to optimize other factors.
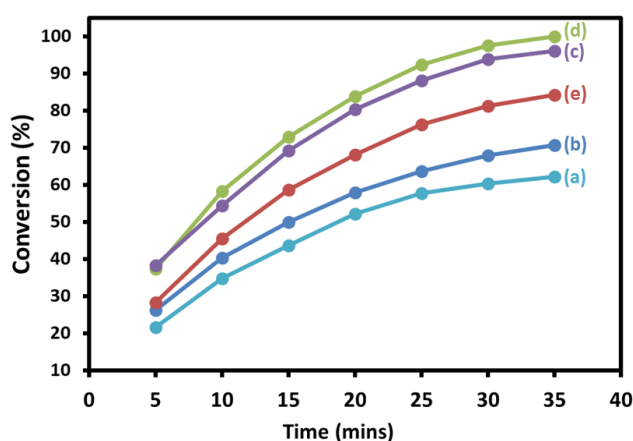
Figure 8. Graphical representation of 1-phenylethanol oxidation using catalyst (**a**) MnO_2–(1%)Ag_2O, (**b**) (1%)HRG/MnO_2–(1%)Ag_2O, (**c**) (3%)HRG/MnO_2–(1%)Ag_2O, (**d**) (5%)HRG/MnO_2–(1%)Ag_2O, and (**e**) (7%)HRG/MnO_2–(1%)Ag_2O.

3.2.2. Impact of Calcination

Calcination process has a strong impact on the structure of the catalyst, including changes in the oxide composition, morphology, and particle size. In addition, the calcination process has profound influence on the catalytic activity of the prepared material. Subsequently, as-prepared nanocomposites are subjected to calcination treatment at 300, 400, and 500 °C. The resulting materials are investigated

for their catalytic efficiency as oxidation catalysts. The results revealed that the catalysts showed high selectivity for acetophenone throughout all oxidation reactions (>99%). Nevertheless, the conversion of 1-phenylethanol was strongly effected by calcination temperature. The catalyst calcined at 300 °C, i.e., (5%)HRG/MnCO$_3$–(1%)Ag$_2$O, exhibited lower catalytic activity, which gave 89.11% of acetophenone from the oxidation of 1-phenylethanol within 25 min (Table 2, entry 4), while in case of 500 °C calcination temperature, i.e., (5%)HRG/Mn$_2$O$_3$–(1%)Ag$_2$O, the alcohol conversion was reduced to 59.74%, which was the least alcohol conversion detected among the catalysts synthesized (Table 2, entry 6). For 400 °C calcination, (5%)HRG/MnO$_2$–(1%)Ag$_2$O exhibits 100% conversion of 1-phenylethanol along with superior specific activity concerning 16 mmol/g·h under similar conditions (Table 2, entry 5).

Table 2. Catalytic oxidation of 1-phenylethanol under different calcination temperatures.

Entry	Catalyst	T. (°C)	SA (m^2/g)	Conv. (%)	Specific Activity (mmol/g·h)	Sel. (%)
1	MnCO$_3$–(1%)Ag$_2$O	300	51.7	58.47	9.36	>99
2	MnO$_2$–(1%)Ag$_2$O	400	84.3	60.39	9.66	>99
3	Mn$_2$O$_3$–(1%)Ag$_2$O	500	41.8	39.81	6.37	>99
4	(5%)HRG/MnCO$_3$–(1%)Ag$_2$O	300	107.1	89.11	14.26	>99
5	(5%)HRG/MnO$_2$–(1%)Ag$_2$O	400	149.1	100.0	16.0	>99
6	(5%)HRG/Mn$_2$O$_3$–(1%)Ag$_2$O	500	98.7	59.74	9.56	>99

Note: Conditions: 2 mmol of 1-phenylethanol, 300 mg catalyst, and 20 mL/min oxygen rate at 100 °C for 25 min.

When the attained results are compared to the catalyst without graphene support, i.e., MnO$_2$–(1%)Ag$_2$O, it was found that under identical circumstances, the alcohol conversion obtained was only 60.39%. The calculated specific activity of the catalyst, i.e., MnO$_2$–(1%)Ag$_2$O, was found to be 9.66 mmol/g·h, which was lower than specific activity of the catalyst containing HRG (Table 2, entry 2). Based on these findings, it is evident that using graphene support improves the efficiency of catalyst significantly. Notably, the obtained catalytic results are consistent with BET surface area data of the synthesized catalyst as well. The catalyst (5%)HRG/MnO$_2$–(1%)Ag$_2$O calcined at 400 °C have the highest surface area among the other temperatures and gave full conversion of 1-phenylethanol. The catalyst heated at 300 and 500 °C, i.e., (5%)HRG/MnCO$_3$–(1%)Ag$_2$O and (5%)HRG/Mn$_2$O$_3$–(1%)Ag$_2$O, respectively, displayed lower 1-phenylethanol conversion and lower surface area. Thus, it can be concluded that the catalytic performance was substantially affected by calcination process. However, acetophenone selectivity was almost independent of surface area of the prepared catalysts. The catalytic results obtained were summarized in Table 2 and presented in Figure 9.
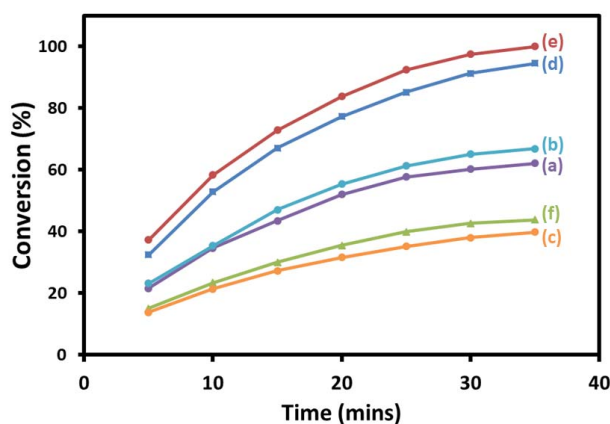
Figure 9. Graphical illustration of aerial oxidation of 1-phenylethanol catalyzed by (**a**) MnCO$_3$–(1%)Ag$_2$O, (**b**) MnO$_2$–(1%)Ag$_2$O, (**c**) Mn$_2$O$_3$–(1%)Ag$_2$O, (**d**) (5%)HRG/MnCO$_3$–(1%)Ag$_2$O, (**e**) Ag$_2$O(1%)–MnO$_2$/(5%)HRG, and (**f**) (5%)HRG/Mn$_2$O$_3$–(1%)Ag$_2$O.
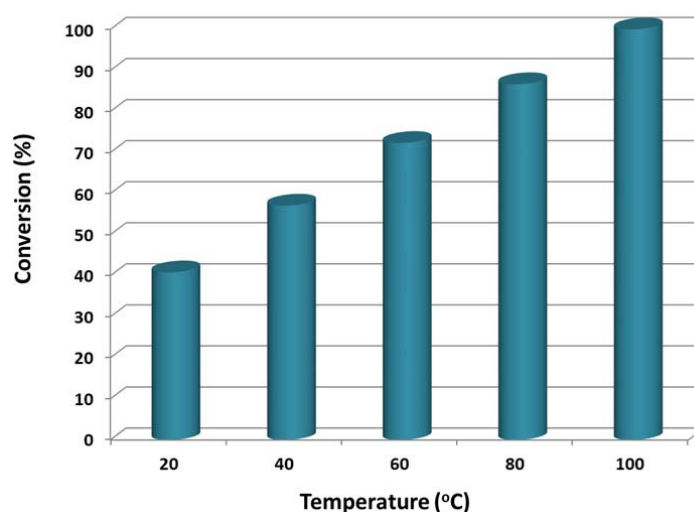
3.2.3. Impact of Reaction Temperature

Usually, the temperature had a pronounced effect on catalytic oxidation of alcohols. Therefore, the influence of temperature during the oxidation of 1-phenylethanol was also assessed by altering the temperature from 20 °C to 100 °C for the aerial oxidation of 1-phenylethanol in presence of (5%)HRG/MnO$_2$–(1%)Ag$_2$O catalyst. The results are compiled in Table 3 and plotted in Figure 10. The attained results reveal that the effectiveness of the present nanocomposite is directly proportional to the reaction temperature, whereas the selectivities toward acetophenone were all as high as >99%. For instance, at low temperature 20 °C, a relatively low alcohol conversion of 33.14% was observed (Table 3, entry 1). As anticipated, high reaction temperature contributed to higher catalytic activity and led to the considerable enhancement of the performance of the prepared catalyst. At high temperature (100 °C), a complete conversion was accomplished under same circumstances (Table 3, entry 5). Thus, the temperature of 100 °C has been chosen for further optimization studies.

Table 3. Influence of temperature on the performance of the synthesized nanocomposite.

Entry	Temperature (°C)	Conv. (%)	Specific Activity (mmol/g·h)	Sel. (%)
1	20	33.14	5.30	>99
2	40	50.20	8.03	>99
3	60	66.41	10.63	>99
4	80	82.93	13.27	>99
5	100	100.0	16.0	>99

Note: Conditions: 300 mg catalyst (5%)HRG/MnO$_2$–(1%)Ag$_2$O calcined at 400 °C, 2 mmol of 1-phenylethanol, and 20 mL/min oxygen rate for 25 min.
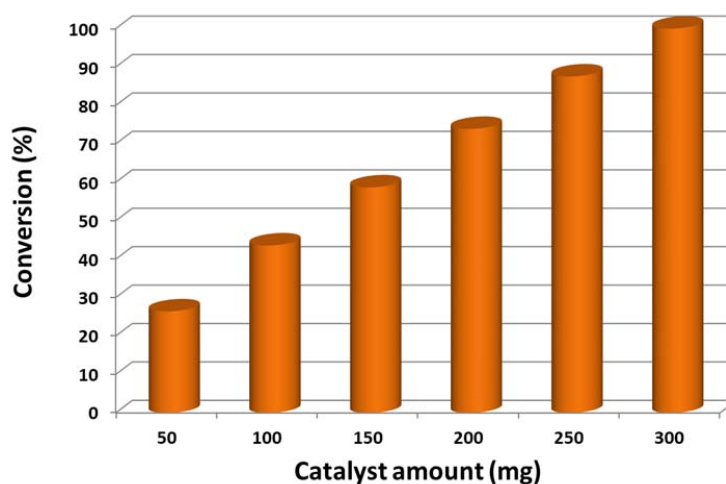

Figure 10. Dependence of 1-phenylethanol conversion on reaction temperature.

3.2.4. Effect of Amount of Catalyst

The role of catalyst quantity during the oxidation process was also examined while keeping other optimized parameters constant, and the attained results are depicted in Figure 11 and compiled in Table 4. It is clear that, by raising the catalyst quantity, the alcohol conversion was also raised gradually, but the selectivity for acetophenone remained unchanged (above 99%). According to Table 4, using a low catalyst amount (50 mg), a poor conversion of 23.06% was obtained, which could be due to fewer active sites (Table 4, entry 1). As anticipated, by raising the catalyst quantity to 100 mg, the 1-phenylethanol conversion also increased to 39.85% (Table 4, entry 2). Further increase in catalyst to 300 mg resulted in the catalyst being afforded excellent efficiency, which produced 100% conversion

with 16.0 mmol/g·h specific activity within 25 min of the reaction (Table 4, entry 5), whilst the rest yielded lower than 100% conversion at similar circumstances. The current study shows that only 3.0 g of the catalyst was required to achieve complete conversion of 1-phenylethanol to acetophenone within 25 min. As seen in Figure 11, the conversion of 1-phenylethanol is directly proportional to the catalyst amount. To ensure the catalytic performance, blank test without the as-fabricated catalyst was conducted under the optimum conditions. No formation of acetophenone was detected by GC, indicating that the prepared catalyst is necessary for this oxidation process.

Figure 11. Conversion of 1-phenylethanol as a function of catalyst (5%)HRG/MnO_2–(1%)Ag_2O amount.

Table 4. Influence of variation of amount of catalyst (5%)HRG/MnO_2–(1%)Ag_2O.

Entry	Catalyst Dosage (mg)	Conv. (%)	Specific Activity (mmol/g·h)	Sel. (%)
1	50	23.06	22.14	>99
2	100	39.85	19.13	>99
3	150	55.12	17.64	>99
4	200	70.81	16.99	>99
5	250	84.70	16.26	>99
6	300	100.0	16.00	>99

Note: Conditions: catalyst (5%)HRG/MnO_2–(1%)Ag_2O calcined at 400 °C, 2 mmol of 1-phenylethanol, and 20 mL/min oxygen rate at 100 °C for 25 min.

3.3. Reusability of Catalyst

The recyclability and stability of the catalyst gained growing interest owing to the fact it is greatly important from both environmental and economic viewpoints. In order to assess the durability and reusability of the (5%)HRG/MnO_2–(1%)Ag_2O catalyst, oxidation of 1-phenylethanol was conducted five consecutive times under optimal conditions, as described in Figure 12. After the complete first oxidation experiment, the catalyst can be easily filtered by simple filtration or centrifugation and washed sequentially with toluene and reused for up to five catalytic reactions. The results, which are illustrated in Figure 12, elucidated no obvious decrease in the performance after five runs. The conversion 1-phenylethanol decreases gradually from 100% to 13.94% after five cycles, presumably due to weight loss during filtration. In the fifth cycle, the selectivity toward acetophenone remained unchanged above 99%. Therefore, the results indicated that the synthesized catalyst possesses excellent reproducibility and stability.
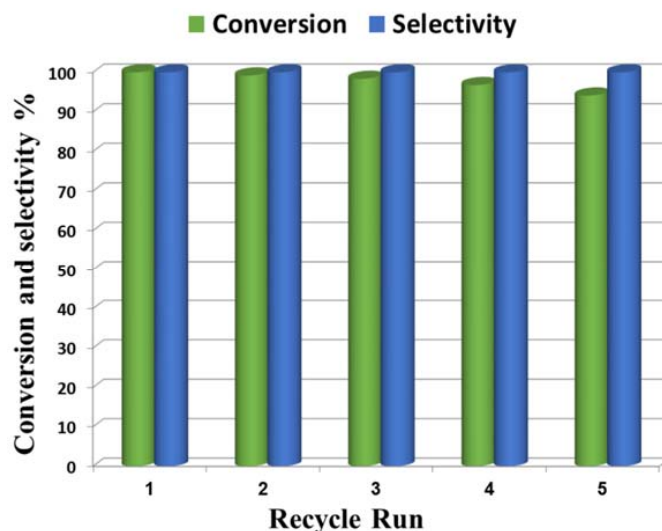
Figure 12. Recycling results of the (5%)HRG/MnO$_2$–(1%)Ag$_2$O catalyst. Conditions: (150 mol %) (5%)HRG/MnO$_2$–(1%)Ag$_2$O calcined at 400 °C, 2 mmol of 1-phenylethanol, and 20 mL/min oxygen rate at 100 °C for 25 min.

The efficiency of our catalytic system was compared with other reported catalysts for 1-phenylethanol oxidation, as illustrated in Table 5. In the present study, the oxidation of 1-phenylethanol to acetophenone is completed in relatively short reaction time (25 min) with more than 99% acetophenone selectivity. Additionally, other catalysts listed take a longer period to complete oxidation of 1-phenylethanol. For example, Karami et al. [55] have prepared palladium NPs dispersed on the surface of polystyrene (Pd NPs/PS) and employed as an oxidation catalyst. The Pd NPs/PS catalyst exhibited complete 1-phenylethanol conversion and more than 99% selectivity for acetophenone after 15 h was obtained with 1.80 mmol/g·h specific activity, which is lower compared to the specific activity (16 mmol/g·h) with 100% conversion and >99 acetophenone selectivity after 25 min in this work. In another example, Reis et al. [56] reported the use of mesoporous niobium phosphate as an oxidation catalyst using H$_2$O$_2$ as an oxidizing agent, but it required very long period 24 h to yield 72% 1-phenylethanol conversion along with lower specific activity (2.74 mmol/g·h) by comparison with the as-prepared (5%)HRG/MnO$_2$–(1%)Ag$_2$O catalyst.

Table 5. A comparison between the efficiency of our catalyst and earlier reported catalysts.

Catalyst	Conv. (%)	Sel. (%)	T (°C)	Time	Specific Activity (mmol/g·h)	Ref.
(5%)HRG/MnO$_2$–(1%)Ag$_2$O	100	>99	100	25 min	16.0	This study
Pd NPs/PS	100	>99	85	15 h	1.80	[55]
NbP-S2	72	100	90	24 h	2.74	[56]
Mo^{VI}O$_2$(bp-bhz)(MeOH)	84.0	-	80	0.5 h	13.77	[57]
15% *w/w* Ag-OMS-2	78.9	-	75	4 h	0.16	[58]
AuCNT	80	-	RT	24 h	-	[59]
VO(ephedrine)$_2$@MNPs	96	>99	80	3 h	9.60	[60]
CoAl$_2$O$_4$	78.54	85.43	80	5 h	1.57	[16]
POM/ZrO$_2$	88	-	RT	3 h	11.73	[61]
Ru/CaO–ZrO$_2$	95	94	90	2 h	7.92	[62]
Pd-pol	98	>99	100	16 h	2.65	[63]
Ru/Mg–LaO	96	>99	80	4 h	2.40	[64]

Table 5. *Cont.*

Catalyst	Conv. (%)	Sel. (%)	T (°C)	Time	Specific Activity (mmol/g·h)	Ref.
FeAPO-5/NaBr	56.2	100	70	8 h	7.45	[65]
2 wt% Ir/TiO$_2$	>99	>99	80	3 h	2.67	[66]
Au/LDH	>99	>99.5	80	2 h	9.28	[67]
Ru/MnO$_x$/CeO$_2$	99	99	27	7 h	1.41	[68]
Au/NiAlO	96	>99	80	1 h	8.0	[69]
PW$_{11}$-DMA$_{16}$/CMPS	92	98.7	90	6 h	2.56	[70]
CoPc@Cell	91	>99	RT	5.5 h	3.31	[71]
Co(II)/ZnO	95	100	70	13 h	1.45	[72]
Fe(NO$_3$)$_3$·9H$_2$O/NHPI	92	>99	RT	48 h	1.92	[73]
Na/CoCl$_3$	99	100	RT	46 h	0.43	[74]
Au/TiO$_2$	100	>99	110	24 h	0.83	[75]
Fe$_3$O$_4$	76	>99	80	18 h	1.40	[76]
FeCl$_3$-imine@SiO$_2$	90	>99	80	6 h	3.26	[77]

3.4. Oxidation of a Various Alcohols over (5%)HRG/MnO$_2$–(1%)Ag$_2$O Catalyst

After optimizing the reaction circumstance, we expanded the oxidation process to the oxidation of a broad range of secondary benzylic and aliphatic alcohols, which also underwent oxidation to give the corresponding ketones; the results are tabulated in Table 6. According to this table, all secondary alcohols were smoothly transformed into the respective ketones with 100% convertibility (Table 6, entries 1–6). Moreover, selectivity towards ketones of more than 99% was achieved. It is worth mentioning that diphenylmethanol was the most reactive among all secondary aromatic alcohol and gave 100% conversion within only 20 min, while 4-chlorobenzhydrol gave 100% conversion after prolonged reaction time, which may be due to 4-chlorobenzhydrol bearing electron-withdrawing group that deactivated the phenyl ring by decreasing the electron density (Table 6, entries 3 and 4). Additionally, 1-phenylethanol and its derivatives also gave 100% conversion in 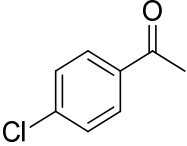short periods (Table 6, entries 1 and 2). Comparatively, aromatic alcohols are more reactive than the aliphatic ones. According to the Table 6, the oxidation of secondary aliphatic alcohols exhibited relatively lower reactivity compared to benzylic ones. For instance, the oxidation of cyclohexanol, 1-buten-3-ol, and 2-octanol to corresponding aliphatic ketones occurred with relatively longer reaction times compared to aromatic ones (Table 6, entries 7–9).

Encouraged by these excellent results, we tried to expand the oxidation process to a broad range of alcohols like primary benzylic, allylic, heterocyclic, and aliphatic alcohols. Fortunately, these alcohols are selectively oxidized to their respective aldehydes employing optimum conditions. It is clear that the catalytic system was found to be also effective for the selective oxidation of primary aromatic alcohols (Table 6, entries 10–22). In addition, selectivity toward aldehydes is more than 99%, because there no over-oxidation to acids occurred, except that the aldehyde was observed. Usually, the oxidation rate of aromatic alcohols with electron-releasing substituents was relatively higher than that of alcohols carrying electron-withdrawing groups. For example, oxidation of an aromatic alcohol-bearing, electron-donating group such 4-methoxybenzyl alcohol gave 100% conversion within 30 min (Table 6, entry 12), while oxidation of alcohol-containing, electron-withdrawing group such as complete oxidation of 4-nitrobenzyl alcohol occurred within longer period (55 min) (Table 6, entry 13). Furthermore, *para*-substituted alcohols gave full oxidation after shorter periods compared to *ortho*- and *meta*-positions, which may be attributed to the fact that *para*-position has lower steric resistance relative to other positions. For example, *para*-methylbenzyl alcohol was fully transformed to its *para*-methylbenzaldehyde within just 30 min (Table 6, entry 11), wheras *meta*- and *ortho*-methylbenzyl alcohol were fully converted to the respective aldehydes after longer times of 40 and 45 min, respectively, in comparison to the *para*-position (Table 6, entries 14 and 15). Additionally, the prepared catalyst was found to be also highly effective towards oxidation of allylic alcohols in the respective aldehydes. For example, cinnamyl alcohol was rapidly transformed to cinnamaldehyde with complete conversion and selectivity within 60 min (Table 6, entry 21). Furthermore, furfuryl alcohol as example of heteroaromatic

alcohols was also completely oxidized to furfural, and more than 99% selectivity towards furfural was obtained in 120 min (Table 6, entry 22). In addition, it is found that the full oxidation of aliphatic alcohols is more difficult than benzylic ones. In this regard, the oxidation of cyclohexanemethanol, 5-Hexen-1-ol, octan-1-ol, and citronellol occurs in slightly longer periods (Table 6, entries 23–26). Based on the above results, it could be deduced that the oxidation of different types of alcohols using (5%)HRG/MnO$_2$–(1%)Ag$_2$O catalyst is strongly affected by steric hindrance and electronic density.

Table 6. Catalytic oxidation of various alcohols over (5%)HRG/MnO$_2$–(1%)Ag$_2$O catalyst.
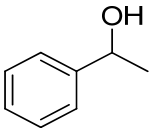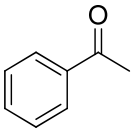
Entry	Substrate	Product	Time (min)	Conv. (%)	Sel. (%)
1			25	100	>99
2			35	100	>99
3			20	100	>99
4			25	100	>99
5			45	100	>99
6			60	100	>99
7			95	100	>99
8			180	100	>99
9			210	100	>99
10			35	100	>99
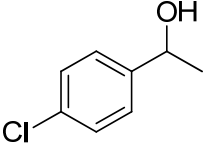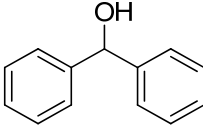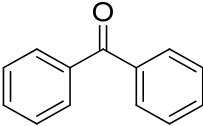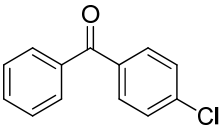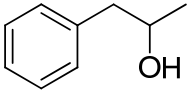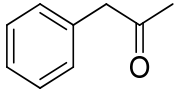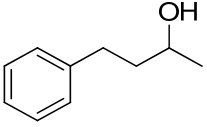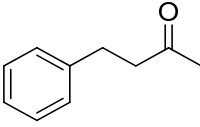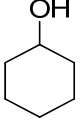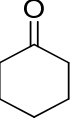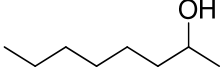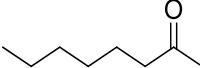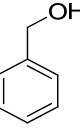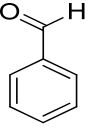
Table 6. *Cont.*

Entry	Substrate	Product	Time (min)	Conv. (%)	Sel. (%)
11			30	100	>99
12			30	100	>99
13			55	100	>99
14			40	100	>99
15			45	100	>99
16			55	100	>99
17			65	100	>99
18			80	100	>99
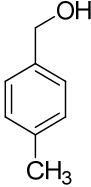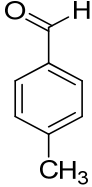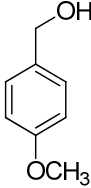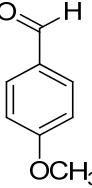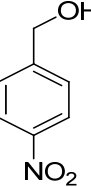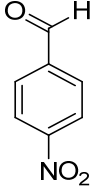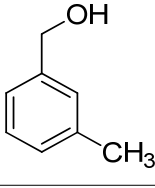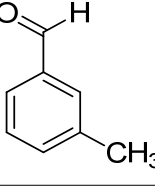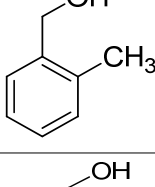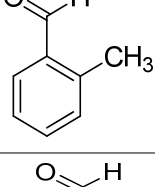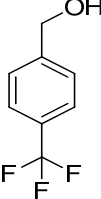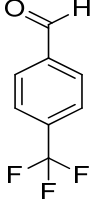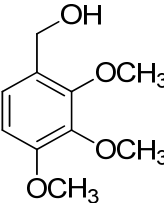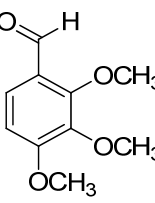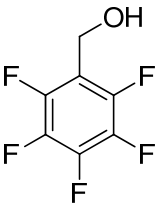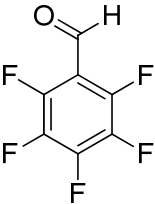
Table 6. *Cont.*

Entry	Substrate	Product	Time (min)	Conv. (%)	Sel. (%)
19			100	100	>99
20			140	100	>99
21			60	100	>99
22			120	100	>99
23			90	100	>99
24			200	100	>99
25			220	100	>99
26			130	100	>99
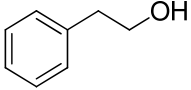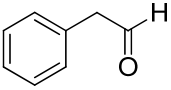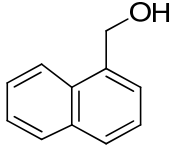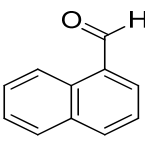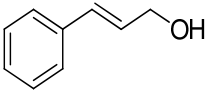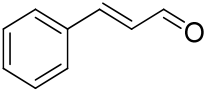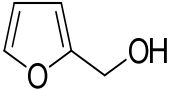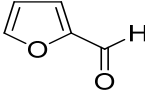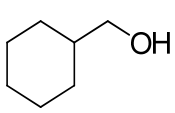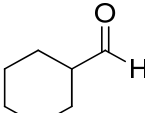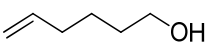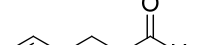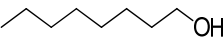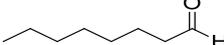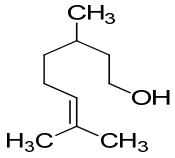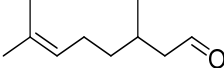
Note: Conditions: as in Figure 12.

4. Conclusions

In summary, we present here an effective, cheap, recyclable, and very mild protocol for the oxidation of alcohols with 100% convertibility and selectivity using Ag_2O NPs-doped MnO_2 immobilized on HRG support as the oxidation catalyst using oxygen as an eco-friendly oxidizing agent. For 1-phenylethanol oxidation as a substrate model, (5%)HRG/MnO_2–(1%)Ag_2O nanocomposite gave higher conversion (100% conversion) than the MnO_2–(1%)Ag_2O catalyst without using graphene support. A full conversion with >99% acetophenone selectivity was accomplished after a short period. The obtained specific activity (16 mmol/g·h) is much higher than that found in earlier publications. Using this catalytic system, various aromatic, allylic, heterocyclic, and aliphatic alcohols can be fully transformed to respective aldehydes and ketones with excellent yields and short reaction times. The current catalytic protocol is highly selective, yielding only desired aldehydes or ketones without further oxidation to acids. The significant advantages of this catalytic system are as follows: (a) straightforward and easy to handle procedure; (b) clean oxidant; (c) not using any additional surfactants and nitrogenous bases; (d) mild circumstances; (e) cheap oxidant and catalyst; (f) full convertibility; (g) complete selectivity; (h) fast reaction; (i) reusable heterogeneous catalyst;

and (j) being applicable to a various types of alcohols. All these advantages will cause this methodology to be very beneficial and applicable to the industrial synthesis of carbonyl compounds.

Author Contributions: S.F.A. and M.E.A. gave the idea of the work; M.E.A., S.F.A., M.K. (Mujeeb Khan), and M.R.S. helped to write the project; M.E.A., M.K. (Mufsir Kuniyil), and M.R.S. performed the experimental section and characterization; and A.A.-W. and M.R.H.S. provided scientific guidance for successful completion of the study and also assisted to write the paper. All authors read and approved the final paper.

Conflicts of Interest: The authors declare no conflict of interest.

References

1. Zhang, G.; Li, S.; Lei, J.; Zhang, G.; Xie, X.; Ding, C.; Liu, R. An efficient biomimetic aerobic oxidation of alcohols catalyzed by iron combined with amino acids. *Synlett* **2016**, *27*, 956–960. [CrossRef]
2. Tojo, G.; Fernández, M.I. *Oxidation of Alcohols to Aldehydes and Ketones: A Guide to Current Common Practice*, 1st ed.; Springer: New York, NY, USA, 2006.
3. Zhu, Y.; Xu, J.; Lu, M. Oxidation of primary and secondary alcohols to the corresponding carbonyl compounds with molecular oxygen using 1, 1-diphenyl-2-picrylhydrazyl and WO_3/Al_2O_3 as catalysts. *Catal. Commun.* **2014**, *48*, 78–84. [CrossRef]
4. Kamimura, A.; Nozaki, Y.; Ishikawa, S.; Inoue, R.; Nakayama, M. K-birnessite MnO_2: A new selective oxidant for benzylic and allylic alcohols. *Tetrahedron Lett.* **2011**, *52*, 538–540. [CrossRef]
5. Patel, S.; Mishra, B. Chromium (VI) oxidants having quaternary ammonium ions: Studies on synthetic applications and oxidation kinetics. *Tetrahedron* **2007**, *63*, 4367–4406. [CrossRef]
6. Arena, F.; Gumina, B.; Lombardo, A.F.; Espro, C.; Patti, A.; Spadaro, L.; Spiccia, L. Nanostructured MnO_x catalysts in the liquid phase selective oxidation of benzyl alcohol with oxygen: Part I. effects of Ce and Fe addition on structure and reactivity. *Appl. Catal. B Environ.* **2015**, *162*, 260–267. [CrossRef]
7. Jiang, N.; Ragauskas, A.J. Vanadium-catalyzed selective aerobic alcohol oxidation in ionic liquid [bmim] PF_6. *Tetrahedron Lett.* **2007**, *48*, 273–276. [CrossRef]
8. Figiel, P.J.; Sobczak, J.M. Mechanistic investigation of the catalytic system based on *N*-hydroxy-phthalimide with vanadium co-catalysts for aerobic oxidation of alcohols with dioxygen. *J. Catal.* **2009**, *263*, 167–172. [CrossRef]
9. Yan, Y.; Jia, X.; Yang, Y. Palladium NPs supported on CNT functionalized by rare-earth oxides for solvent-free aerobic oxidation of benzyl alcohol. *Catal. Today* **2016**, *259*, 292–302. [CrossRef]
10. Chibani, S.; Michel, C.; Delbecq, F.; Pinel, C.; Besson, M. On the key role of hydroxyl groups in platinum-catalysed alcohol oxidation in aqueous medium. *Catal. Sci. Technol.* **2013**, *3*, 339–350. [CrossRef]
11. Wang, T.; Yuan, X.; Li, S.; Zeng, L.; Gong, J. CeO_2-modified Au@ SBA-15 nanocatalysts for liquid-phase selective oxidation of benzyl alcohol. *Nanoscale* **2015**, *7*, 7593–7602. [CrossRef] [PubMed]
12. Cheung, W.-H.; Yu, W.-Y.; Yip, W.-P.; Zhu, N.-Y.; Che, C.-M. A silica gel-supported ruthenium complex of 1, 4, 7-trimethyl-1, 4, 7-triazacyclononane as recyclable catalyst for chemoselective oxidation of alcohols and alkenes by *tert*-butyl hydroperoxide. *J. Org. Chem.* **2002**, *67*, 7716–7723. [CrossRef] [PubMed]
13. Xie, M.; Dai, X.; Meng, S.; Fu, X.; Chen, S. Selective oxidation of aromatic alcohols to corresponding aromatic aldehydes using In_2S_3 microsphere catalyst under visible light irradiation. *Chem. Eng. J.* **2014**, *245*, 107–116. [CrossRef]
14. Das, O.; Paine, T.K. Aerobic oxidation of primary alcohols catalyzed by copper complexes of 1, 10-phenanthroline-derived ligands. *Dalton Trans.* **2012**, *41*, 11476–11481. [CrossRef] [PubMed]
15. Hajipour, A.R.; Karimi, H.; Koohi, A. Selective oxidation of alcohols over nickel zirconium phosphate. *Chin. J. Catal.* **2015**, *36*, 1109–1116. [CrossRef]
16. Ragupathi, C.; Vijaya, J.J.; Narayanan, S.; Jesudoss, S.; Kennedy, L.J. Highly selective oxidation of benzyl alcohol to benzaldehyde with hydrogen peroxide by cobalt aluminate catalysis: A comparison of conventional and microwave methods. *Ceram. Int.* **2015**, *41*, 2069–2080. [CrossRef]

17. Wang, N.; Liu, R.; Chen, J.; Liang, X. NaNO$_2$-activated, iron–TEMPO catalyst system for aerobic alcohol oxidation under mild conditions. *Chem. Commun.* **2005**, *14*, 5322–5324. [CrossRef] [PubMed]

18. Goh, T.W.; Xiao, C.; Maligal-Ganesh, R.V.; Li, X.; Huang, W. Utilizing mixed-linker zirconium based metal-organic frameworks to enhance the visible light photocatalytic oxidation of alcohol. *Chem. Eng. Sci.* **2015**, *124*, 45–51. [CrossRef]

19. Forouzani, M.; Mardani, H.R.; Ziari, M.; Malekzadeh, A.; Biparva, P. Comparative study of oxidation of benzyl alcohol: Influence of Cu-doped metal cation on nano ZnO catalytic activity. *Chem. Eng. J.* **2015**, *275*, 220–226. [CrossRef]

20. Ndolomingo, M.J.; Meijboom, R. Selective liquid phase oxidation of benzyl alcohol to benzaldehyde by *tert*-butyl hydroperoxide over γ-Al$_2$O$_3$ supported copper and gold NPs. *Appl. Surf. Sci.* **2017**, *398*, 19–32. [CrossRef]

21. Bhaumik, C.; Stein, D.; Vincendeau, S.; Poli, R.; Manoury, É. Oxidation of alcohols by TBHP in the presence of sub-stoichiometric amounts of MnO$_2$. *C. R. Chim.* **2016**, *19*, 566–570. [CrossRef]

22. Adil, S.F.; Alabbad, S.; Kuniyil, M.; Khan, M.; Alwarthan, A.; Mohri, N.; Tremel, W.; Tahir, M.N.; Siddiqui, M.R.H. Vanadia supported on nickel manganese oxide nanocatalysts for the catalytic oxidation of aromatic alcohols. *Nanoscale Res. Lett.* **2015**, *10*, 52. [CrossRef] [PubMed]

23. Elmaci, G.; Ozer, D.; Zumreoglu-Karan, B. Liquid phase aerobic oxidation of benzyl alcohol by using manganese ferrite supported-manganese oxide nanocomposite catalyst. *Catal. Commun.* **2017**, *89*, 56–59. [CrossRef]

24. Mondal, A.; Jana, N.R. Surfactant-free, stable noble metal–graphene nanocomposite as high performance electrocatalyst. *ACS Catal.* **2014**, *4*, 593–599. [CrossRef]

25. Geim, A.K.; Novoselov, K.S. The rise of graphene. *Nat. Mater.* **2007**, *6*, 183–191. [CrossRef] [PubMed]

26. Allen, M.J.; Tung, V.C.; Kaner, R.B. Honeycomb carbon: A review of graphene. *Chem. Rev.* **2010**, *110*, 132–145. [CrossRef] [PubMed]

27. Khan, M.; Tahir, M.N.; Adil, S.F.; Khan, H.U.; Siddiqui, M.R.H.; Al-warthan, A.A.; Tremel, W. Graphene based metal and metal oxide nanocomposites: Synthesis, properties and their applications. *J. Mater. Chem. A* **2015**, *3*, 18753–18808. [CrossRef]

28. Singh, V.; Joung, D.; Zhai, L.; Das, S.; Khondaker, S.I.; Seal, S. Graphene based materials: Past, present and future. *Prog. Mater. Sci.* **2011**, *56*, 1178–1271. [CrossRef]

29. Tang, M.; Wang, X.; Wu, F.; Liu, Y.; Zhang, S.; Pang, X.; Li, X.; Qiu, H. Au nanoparticle/graphene oxide hybrids as stabilizers for pickering emulsions and Au nanoparticle/graphene oxide@ polystyrene microspheres. *Carbon* **2014**, *71*, 238–248. [CrossRef]

30. Al-Marri, A.H.; Khan, M.; Shaik, M.R.; Mohri, N.; Adil, S.F.; Kuniyil, M.; Alkhathlan, H.Z.; Al-Warthan, A.; Tremel, W.; Tahir, M.N. Green synthesis of Pd@ graphene nanocomposite: Catalyst for the selective oxidation of alcohols. *Arab. J. Chem.* **2016**, *9*, 835–845. [CrossRef]

31. Dreyer, D.R.; Jia, H.P.; Bielawski, C.W. Graphene oxide: A convenient carbocatalyst for facilitating oxidation and hydration reactions. *Angew. Chem. Int. Ed.* **2010**, *49*, 6813–6816. [CrossRef]

32. Zahed, B.; Hosseini-Monfared, H. A Comparative study of silver-graphene oxide nanocomposites as a recyclable catalyst for the aerobic oxidation of benzyl alcohol: Support effect. *Appl. Surf. Sci.* **2015**, *328*, 536–547. [CrossRef]

33. Zhu, J.; Carabineiro, S.A.; Shan, D.; Faria, J.L.; Zhu, Y.; Figueiredo, J.L. Oxygen activation sites in gold and iron catalysts supported on carbon nitride and activated carbon. *J. Catal.* **2010**, *274*, 207–214. [CrossRef]

34. Chua, C.K.; Pumera, M. Chemical reduction of graphene oxide: A synthetic chemistry viewpoint. *Chem. Soc. Rev.* **2014**, *43*, 291–312. [CrossRef] [PubMed]

35. Yoo, E.; Okata, T.; Akita, T.; Kohyama, M.; Nakamura, J.; Honma, I. Enhanced electrocatalytic activity of Pt subnanoclusters on graphene nanosheet surface. *Nano Lett.* **2009**, *9*, 2255–2259. [CrossRef] [PubMed]

36. Miao, M.; Feng, J.; Jin, Q.; He, Y.; Liu, Y.; Du, Y.; Zhang, N.; Li, D. Hybrid Ni–Al layered double hydroxide/graphene composite supported gold NPs for aerobic selective oxidation of benzyl alcohol. *RSC Adv.* **2015**, *5*, 36066–36074. [CrossRef]

37. Shinde, V.M.; Skupien, E.; Makkee, M. Synthesis of highly dispersed Pd NPs supported on multi-walled carbon nanotubes and their excellent catalytic performance for oxidation of benzyl alcohol. *Catal. Sci. Technol.* **2015**, *5*, 4144–4153. [CrossRef]

38. Yang, S.; Lin, Y.; Song, X.; Zhang, P.; Gao, L. Covalently coupled ultrafine H-TiO$_2$ nanocrystals/nitrogen-doped graphene hybrid materials for high-performance supercapacitor. *ACS Appl. Mater. Interfaces* **2015**, *7*, 17884–17892. [CrossRef] [PubMed]

39. Mondal, P.; Salam, N.; Mondal, A.; Ghosh, K.; Tuhina, K.; Islam, S.M. A highly active recyclable gold–graphene nanocomposite material for oxidative esterification and Suzuki cross-coupling reactions in green pathway. *J. Colloid Interface Sci.* **2015**, *459*, 97–106. [CrossRef] [PubMed]

40. Mirza-Aghayan, M.; Tavana, M.M.; Boukherroub, R. Palladium NPs supported on reduced graphene oxide as an efficient catalyst for the reduction of benzyl alcohol compounds. *Catal. Commun.* **2015**, *69*, 97–103. [CrossRef]

41. Qusti, A.; Mohamed, R.; Salam, M.A. Photocatalytic synthesis of aniline from nitrobenzene using Ag-reduced graphene oxide nanocomposite. *Ceram. Int.* **2014**, *40*, 5539–5546. [CrossRef]

42. Zhao, B.; Liu, J.; Zhou, L.; Long, D.; Feng, K.; Sun, X.; Zhong, J. Probing the electronic structure of M-graphene oxide (M = Ni, Co, NiCo) catalysts for hydrolytic dehydrogenation of ammonia borane. *Appl. Surf. Sci.* **2016**, *362*, 79–85. [CrossRef]

43. Yang, Y.; Luo, L.-M.; Guo, Y.-F.; Dai, Z.-X.; Zhang, R.-H.; Sun, C.; Zhou, X.-W. In situ synthesis of PtPd bimetallic nanocatalysts supported on graphene nanosheets for methanol oxidation using triblock copolymer as reducer and stabilizer. *J. Electroanal. Chem.* **2016**, *783*, 132–139. [CrossRef]

44. Wu, G.; Wang, X.; Guan, N.; Li, L. Palladium on graphene as efficient catalyst for solvent-free aerobic oxidation of aromatic alcohols: Role of graphene support. *Appl. Catal. B Environ.* **2013**, *136*, 177–185. [CrossRef]

45. Hu, Z.; Zhao, Y.; Liu, J.; Wang, J.; Zhang, B.; Xiang, X. Ultrafine MnO$_2$ NPs decorated on graphene oxide as a highly efficient and recyclable catalyst for aerobic oxidation of benzyl alcohol. *J. Colloid Interface Sci.* **2016**, *483*, 26–33. [CrossRef] [PubMed]

46. Yu, X.; Huo, Y.; Yang, J.; Chang, S.; Ma, Y.; Huang, W. Reduced graphene oxide supported Au NPs as an efficient catalyst for aerobic oxidation of benzyl alcohol. *Appl. Surf. Sci.* **2013**, *280*, 450–455. [CrossRef]

47. Wu, X.; Guo, S.; Zhang, J. Au/graphene quantum dots/ferroferric oxide composites as catalysts for the solvent-free oxidation of alcohols. *Mater. Lett.* **2016**, *183*, 227–231. [CrossRef]

48. Siddiqui, M.R.H.; Warad, I.; Adil, S.; Mahfouz, R.; Al-Arifi, A. Nano-gold supported nickel manganese oxide: Synthesis, characterisation and evaluation as oxidation catalyst. *Oxid. Commun.* **2012**, *35*, 476–481.

49. Alabbad, S.; Adil, S.; Assal, M.; Khan, M.; Alwarthan, A.; Siddiqui, M.R.H. Gold & silver NPs supported on manganese oxide: Synthesis, characterization and catalytic studies for selective oxidation of benzyl alcohol. *Arab. J. Chem.* **2014**, *7*, 1192–1198.

50. Assal, M.E.; Kuniyil, M.; Khan, M.; Al-Warthan, A.; Siddiqui, M.R.H.; Tremel, W.; Nawaz Tahir, M.; Adil, S.F. Synthesis and comparative catalytic study of Zirconia–MnCO$_3$ or –Mn$_2$O$_3$ for the oxidation of benzylic alcohols. *Chem. Open* **2016**, *6*, 112–120.

51. Hummers, W.S., Jr.; Offeman, R.E. Preparation of graphitic oxide. *J. Am. Chem. Soc.* **1958**, *80*, 1339. [CrossRef]

52. Assal, M.E.; Shaik, M.R.; Kuniyil, M.; Khan, M.; Al-Warthan, A.; Siddiqui, M.R.H.; Khan, S.M.; Tremel, W.; Tahir, M.N.; Adil, S.F. A highly reduced graphene oxide/ZrO$_x$–MnCO$_3$ or–Mn$_2$O$_3$ nanocomposite as an efficient catalyst for selective aerial oxidation of benzylic alcohols. *RSC Adv.* **2017**, *7*, 55336–55349. [CrossRef]

53. Esrafili, M.D.; Nematollahi, P.; Abdollahpour, H. A comparative DFT study on the CO oxidation reaction over Al-and Ge-embedded graphene as efficient metal-free catalysts. *Appl. Surf. Sci.* **2016**, *378*, 418–425. [CrossRef]

54. Assal, M.E.; Shaik, M.R.; Kuniyil, M.; Khan, M.; Venkata, S.J.; Alzahrani, A.Y.; Al-Warthan, A.; Al-Tamrah, S.A.; Siddiqui, M.R.H.; Hashmi, S.A.; et al. Silver-doped manganese based nanocomposites for aerial oxidation of alcohols. *Mater. Express* **2018**, *8*, 35–54. [CrossRef]

55. Karami, K.; Ghasemi, M.; Naeini, N.H. Palladium NPs supported on polymer: An efficient and reusable heterogeneous catalyst for the Suzuki cross-coupling reactions and aerobic oxidation of alcohols. *Catal. Commun.* **2013**, *38*, 10–15. [CrossRef]

56. Reis, M.C.; Barros, S.D.; Lachter, E.R.; San Gil, R.A.; Flores, J.H.; da Silva, M.I.P.; Onfroy, T. Synthesis, characterization and catalytic activity of meso-niobium phosphate in the oxidation of benzyl alcohols. *Catal. Today* **2012**, *192*, 117–122. [CrossRef]

57. Maurya, M.R.; Saini, N.; Avecilla, F. Catalytic oxidation of secondary alcohols by molybdenum complexes derived from 4-acyl pyrazolone in presence and absence of an N-based additive: Conventional versus microwave assisted method. *Inorg. Chim. Acta* **2015**, *438*, 168–178. [CrossRef]

58. Yadav, G.D.; Yadav, A.R. Selective liquid phase oxidation of secondary alcohols into ketones by *tert*-butyl hydroperoxide on nano-fibrous Ag-OMS-2 catalyst. *J. Mol. Catal. A Chem.* **2013**, *380*, 70–77. [CrossRef]

59. Kumar, R.; Gravel, E.; Hagege, A.; Li, H.; Jawale, D.V.; Verma, D.; Namboothiri, I.N.; Doris, E. Carbon nanotube–gold nanohybrids for selective catalytic oxidation of alcohols. *Nanoscale* **2013**, *5*, 6491–6497. [CrossRef] [PubMed]

60. Rostami, A.; Pourshiani, O.; Darvishi, N.; Atashkar, B. Efficient and green oxidation of alcohols with tert-butyl hydrogenperoxide catalyzed by a recyclable magnetic core-shell nanoparticle-supported oxo-vanadium ephedrine complex. *C. R. Chim.* **2017**, *20*, 435–439. [CrossRef]

61. Farhadi, S.; Zaidi, M. Polyoxometalate–zirconia (POM/ZrO_2) nanocomposite prepared by sol–gel process: A green and recyclable photocatalyst for efficient and selective aerobic oxidation of alcohols into aldehydes and ketones. *Appl. Catal. A* **2009**, *354*, 119–126. [CrossRef]

62. Yasu-eda, T.; Kitamura, S.; Ikenaga, N.-O.; Miyake, T.; Suzuki, T. Selective oxidation of alcohols with molecular oxygen over Ru/CaO–ZrO_2 catalyst. *J. Mol. Catal. A Chem.* **2010**, *323*, 7–15. [CrossRef]

63. Dell'Anna, M.M.; Mali, M.; Mastrorilli, P.; Cotugno, P.; Monopoli, A. Oxidation of benzyl alcohols to aldehydes and ketones under air in water using a polymer supported palladium catalyst. *J. Mol. Catal. A Chem.* **2014**, *386*, 114–119. [CrossRef]

64. Kantam, M.L.; Reddy, R.S.; Pal, U.; Sudhakar, M.; Venugopal, A.; Ratnam, K.J.; Figueras, F.; Chintareddy, V.R.; Nishina, Y. Ruthenium/magnesium–lanthanum mixed oxide: An efficient reusable catalyst for oxidation of alcohols by using molecular oxygen. *J. Mol. Catal. A Chem.* **2012**, *359*, 1–7. [CrossRef]

65. Qi, L.; Qi, X.; Wang, J.; Zheng, L. A synergistic effect in the combination of H_2O_2, FeAPO-5 and NaBr for selective oxidation of benzyl alcohols. *Catal. Commun.* **2011**, *16*, 225–228. [CrossRef]

66. Yoshida, A.; Mori, Y.; Ikeda, T.; Azemoto, K.; Naito, S. Enhancement of catalytic activity of Ir/TiO_2 by partially reduced titanium oxide in aerobic oxidation of alcohols. *Catal. Today* **2013**, *203*, 153–157. [CrossRef]

67. Wang, L.; Meng, X.; Xiao, F. Au NPs supported on a layered double hydroxide with excellent catalytic properties for the aerobic oxidation of alcohols. *Chin. J. Catal.* **2010**, *31*, 943–947. [CrossRef]

68. Sato, T.; Komanoya, T. Selective oxidation of alcohols with molecular oxygen catalyzed by $Ru/Mnox/CeO_2$ under mild conditions. *Catal. Commun.* **2009**, *10*, 1095–1098. [CrossRef]

69. Zhao, J.; Yu, G.; Xin, K.; Li, L.; Fu, T.; Cui, Y.; Liu, H.; Xue, N.; Peng, L.; Ding, W. Highly active gold catalysts loaded on NiAl-oxide derived from layered double hydroxide for aerobic alcohol oxidation. *Appl. Catal. A* **2014**, *482*, 294–299. [CrossRef]

70. Wang, H.; Fang, L.; Yang, Y.; Hu, R.; Wang, Y. Immobilization $Na_7PW_{11}O_{39}$ on quanternary ammonium functionalized chloromethylated polystyrene by electrostatic interactions: An efficient recyclable catalyst for alcohol oxidation. *Appl. Catal. A* **2016**, *520*, 35–43. [CrossRef]

71. Shaabani, A.; Keshipour, S.; Hamidzad, M.; Shaabani, S. Cobalt (II) phthalocyanine covalently anchored to cellulose as a recoverable and efficient catalyst for the aerobic oxidation of alkyl arenes and alcohols. *J. Mol. Catal. A Chem.* **2014**, *395*, 494–499. [CrossRef]

72. Hou, J.; Luan, Y.; Tang, J.; Wensley, A.M.; Yang, M.; Lu, Y. Synthesis of UiO-66-NH$_2$ derived heterogeneous copper (II) catalyst and study of its application in the selective aerobic oxidation of alcohols. *J. Mol. Catal. A Chem.* **2015**, *407*, 53–59. [CrossRef]

73. Zhao, H.; Sun, W.; Miao, C.; Zhao, Q. Aerobic oxidation of secondary alcohols using NHPI and iron salt as catalysts at room temperature. *J. Mol. Catal. A Chem.* **2014**, *393*, 62–67. [CrossRef]

74. Zhou, L.-H.; Yu, X.-Q.; Pu, L. Na-promoted aerobic oxidation of alcohols to ketones. *Tetrahedron Lett.* **2010**, *51*, 475–477. [CrossRef]

75. Vindigni, F.; Dughera, S.; Armigliato, F.; Chiorino, A. Aerobic oxidation of alcohols on Au/TiO_2 catalyst: New insights on the role of active sites in the oxidation of primary and secondary alcohols. *Monatsh. Chem.* **2016**, *147*, 391–403. [CrossRef]

76. Shaikh, M.; Satanami, M.; Ranganath, K.V. Efficient aerobic oxidation of alcohols using magnetically recoverable catalysts. *Catal. Commun.* **2014**, *54*, 91–93. [CrossRef]

77. Sahu, D.; Silva, A.R.; Das, P. A novel iron (III)-based heterogeneous catalyst for aqueous oxidation of alcohols using molecular oxygen. *RSC Adv.* **2015**, *5*, 78553–78560. [CrossRef]